Author(s): von Boehm, Juhani & Nieminen, Risto M.

Title: Molecular-dynamics study of partial edge dislocations in copper and gold: Interactions, structures, and self-diffusion

Year: 1996

Version: Final published version

Please cite the original version:

von Boehm, Juhani & Nieminen, Risto M. 1996. Molecular-dynamics study of partial edge dislocations in copper and gold: Interactions, structures, and self-diffusion. Physical Review B. Volume 53, Issue 14. 8956-8966. ISSN 1550-235X (electronic). DOI: 10.1103/physrevb.53.8956.

Molecular-dynamics study of partial edge dislocations in copper and gold: Interactions, structures, and self-diffusion

Juhani von Boehm
Laboratory of Computational Dynamics, Helsinki University of Technology, 02150 Espoo, Finland

Risto M. Nieminen
Laboratory of Physics, Helsinki University of Technology, 02150 Espoo, Finland
(Received 6 November 1995)

The interactions between the [112] partial dislocations (PD), the interactions of vacancies and interstitials with the PD and their structures near the PD, as well as self-diffusion along the PD's in copper and gold are studied by using constant-*NTV* (number of atoms, temperature, and volume) molecular dynamics and the Ackland-Tichy-Vitek-Finnis many-atom interaction model. The interaction energy between the PD's is found to agree accurately with the elastic-continuum energy beyond and at the equilibrium separation distance whereas the former energy grows much more strongly at smaller separation distances due to the increased core repulsion. This behavior indicates a small core overlap at the equilibrium. A vacancy at the edge of a PD is found to have a form of a distorted hexagon whereas an interstitial is found to form a long $\langle 110 \rangle$ crowdion in the $(11\bar{1})$ plane in front of the edge of a PD for both metals. The self-diffusion activation energy for the vacancy mechanism is found to be at least 0.33 eV smaller than that for the interstitial mechanism in the region of the PD pair in gold whereas the corresponding activation energies are estimated to be equal in copper. We find that self-diffusion has nearly equal components along the edges of the PD's and the stacking fault ribbon. This can explain why self-diffusion in metals has a tendency to be weaker along PD pairs than along perfect dislocations.

I. INTRODUCTION

Dislocations play a central role in many of the basic phenomena of materials such as in plastic deformation, in mass transport as fast diffusion channels, in the process of melting, and in the formation and propagation of cracks under applied force.[1,2] A thorough understanding of these phenomena rests ultimately on the knowledge of the atomic properties of dislocations. Experiments (like electron microscopy and positron annihilation) can give only indirect information of these properties, making molecular dynamics (MD) simulations[3] a valuable approach in this context. The present paper deals with edge dislocations in the face-centered cubic (fcc) metals copper and gold. The energetically most favorable edge dislocations appear in the [112] direction as pairs of Shockley partial dislocations with a hexagonal close-packed (hcp) stacking fault ribbon in between.[1] In this case the whole region consisting of the two partial dislocations, the hcp stacking fault ribbon and the close surroundings are of principal interest. We call this region simply the dislocation region (DR). The MD studies of the interactions between the partial dislocations, the structures of the DR, the interactions of point defects (vacancies, interstitials) with a partial dislocation and the structures of point defects in the DR are still relatively scarce.[4–11]

At higher temperatures enhanced self-diffusion (also called pipe-diffusion) occurs along partial dislocation pairs. The usual tracer diffusion experiments along low-angle grain boundaries[12] are not able to give information about the main mechanism of self-diffusion. According to an argument by Friedel,[1] self-diffusion should be due to vacancies because interstitials may be expected to find sites close to the partial dislocations where they will be more stable than in the bulk. Another argument for the vacancy mechanism is the fact that the activation energy for the interstitial mechanism is significantly larger than that for the vacancy mechanism in the bulk, and the vicinity of a partial dislocation is not expected to reduce this difference sufficiently. The majority of later studies prefer the vacancy mechanism[5,12] whereas a recent MD simulation for copper gave the interesting variant result that vacancies and interstitials contribute comparably to self-diffusion.[10,11]

Another more general problem related to self-diffusion along dislocations is as follows. It has been found experimentally that in metals self-diffusion has a tendency to be weaker along partial dislocations than along perfect dislocations.[12] This is attributed either to the decreased Burgers vector of the partial dislocations[12] or to the spread of self-diffusion into the whole DR.[13] The MD simulation for copper favors the latter explanation.[10,11]

In the case of fcc metals the traditional pair-potential approximation (PPA) suffers from several deficiencies.[14] The Cauchy ratio C_{12}/C_{44} in the PPA equals 1, whereas in reality it equals 1.5 for copper and 3.7 for gold. Other deficiencies are the overestimations of the vacancy formation energy and the melting temperature. To improve the description of these properties we use the Ackland-Tichy-Vitek-Finnis (ATVF) (Ref. 15) many-atom interaction model in this paper.

The purpose of this paper is to study the atomic properties of the DR (interactions between partial dislocations, interactions of vacancies and interstitials with a partial dislocation as well as their structures) and self-diffusion along the [112] partial dislocation pair in copper and gold using MD simulation. The format of this paper is as follows. The methods

are briefly presented in Sec. II. The geometry and the initialization of the [112] partial dislocation pair are explained in Sec. III. The results of the atomic properties and self-diffusion are presented and discussed in Sec. IV and V, respectively. The conclusions are drawn in Sec. VI. Some parts of this paper have appeared in short reports elsewhere.[8,9,16]

II. METHODS

A. Molecular dynamics

We use the Nosé-Hoover constant-NTV MD method[17–20] in this paper (N, T, and V stand for the number of atoms, temperature, and volume, respectively). The equations of motion in real variables for a monatomic system are

$$\frac{d^2\mathbf{r}_i}{dt^2}=\frac{1}{m}\,\mathbf{f}_i-\xi\mathbf{v}_i\,, \tag{1}$$

$$\dot{\xi}\equiv\frac{d\xi}{dt}=\frac{1}{Q}\left\{\sum_i\, m\mathbf{v}_i^2-n_f k_B T\right\}, \tag{2}$$

where $\mathbf{r}_i$, m, $\mathbf{f}_i$, and $\mathbf{v}_i$ denote the position, mass, total force, and velocity of nucleus i, respectively, ξ is the friction coefficient controlling temperature T, Q is the thermal inertia parameter, n_f denotes the number of degrees of freedom, and k_B is Boltzmann's constant. We use a generalized velocity-Verlet algorithm[3,21] to solve Eqs. (1) and (2) (see the Appendix). In the thermal inertia parameter[22] $Q=n_f k_B T\tau^2$ the thermal relaxation time τ equals 4–10 fs during transients (when the value of the temperature T is changed) and 10–40 fs for equilibrated systems.

The ATVF total potential energy is[15]

$$\mathscr{V}(N)=\frac{1}{2}\sum_{\substack{i,j=1\\(i\neq j)}}^{N}\Phi(|\mathbf{r}_i-\mathbf{r}_j|)+\sum_{i=1}^{N}U(n_i) \tag{3}$$

and the ATVF force $\mathbf{f}_i$ in Eq. (1) is

$$\mathbf{f}_i=-\nabla_i\mathscr{V}=-\sum_{\substack{j\\(j\neq i)}}\{\Phi'(|\mathbf{r}_i-\mathbf{r}_j|)+[U'(n_i)+U'(n_j)]\rho'(|\mathbf{r}_i-\mathbf{r}_j|)\}\,\frac{\mathbf{r}_i-\mathbf{r}_j}{|\mathbf{r}_i-\mathbf{r}_j|}, \tag{4}$$

where

$$U(n_i)=-\sqrt{n_i} \tag{5}$$

and

$$n_i=\sum_{\substack{j=1\\(j\neq i)}}^{N}\rho(|\mathbf{r}_i-\mathbf{r}_j|). \tag{6}$$

In Eqs. (4)–(6) the prime denotes a derivative with respect to the argument, Φ is the repulsive pair-potential, U is the attractive many-atom potential, n_i is the second moment of the electronic density of states, and ρ is an empirical short range radial function.

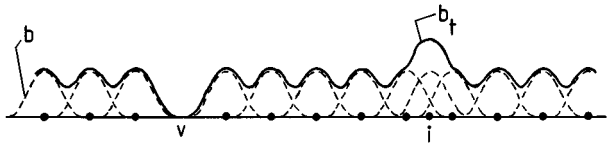

FIG. 1. One-dimensional presentation of the coordination density b_t (solid line) composed of the bell-shaped atomic densities b (dashed lines) according to Eqs. (7) and (8). The symbols v and i denote a vacancy and an interstitial, respectively.

B. Migration

To monitor the migration of individual vacancies and interstitials in the DR we have developed the following *coordination density* method. In this method a bell-shaped density profile of the form

$$b(r)=\left[1-2\left(\frac{r}{c}\right)^2+\left(\frac{r}{c}\right)^4\right]\theta(c-r) \tag{7}$$

is placed at each atom (the constant c is somewhat larger than half the nearest-neighbor separation and equals 3.0 Å for copper and 3.5 Å for gold, r is the distance from the nucleus, and θ is the Heaviside step function). The coordination density b_t is calculated as the sum of the atomic contributions:

$$b_t(\mathbf{r})=\sum_{i=1}^{N}b(|\mathbf{r}-\mathbf{r}_i|). \tag{8}$$

The minimum of b_t locates a vacancy provided that this minimum is lower than a typical minimum value of b_t in a regular crystal (Fig. 1). The vacancy is surrounded by a sphere of radius R plus a "skin." b_t is calculated in a grid with intervals $R/10$ inside the sphere from the atoms inside the "sphere plus skin" region. The maximum of b_t locates the interstitial atom provided that this maximum is larger than a typical maximum value of b_t in a regular crystal (see Fig. 1). The interstitial nucleus is also surrounded by a sphere of radius R plus a "skin" but b_t is now calculated only at the nuclei inside the sphere. The method is advantageous for migration studies because it takes automatically into account all processes where the interstitial role is transferred from one atom to a neighbor atom.

As the second method we calculate the net mass transport induced by a vacancy or an interstitial in the DR using the definition of the diffusion constant

$$D(N)=\lim_{t\to\infty}\frac{1}{6t}\sum_{i=1}^{N}[\mathbf{r}_i(t)-\mathbf{r}_i(0)]^2. \tag{9}$$

The convergence properties of D are studied using the related quantities

$$\frac{1}{t}R_\alpha^2=\frac{1}{t}\sum_i\,[\mathbf{r}_{i\alpha}(t)-\mathbf{r}_{i\alpha}(0)]^2,\quad \alpha=x,y,z. \tag{10}$$

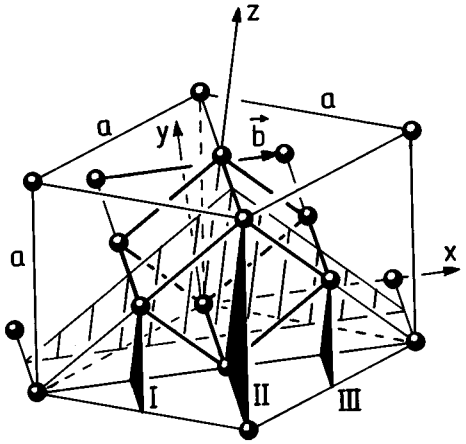

FIG. 2. Face-centered cubic crystal structure. a is the length of a side of the cube and **b** the Burgers vector of a perfect [112] edge dislocation. x, y, and z denote the Cartesian coordinate axes used in the calculations. The z axis is the edge of the perfect dislocation. The atomic half-planes I, II, and III indicated with black areas are used in the Cotterill-Doyama recipe (see the text). The shaded plane is the (imagined) $(11\bar{1})$ slip plane.

III. INITIAL GEOMETRY OF THE [112] PARTIAL DISLOCATION PAIR

The fcc crystal structure is shown in Fig. 2. The formation of an [112] edge dislocation (coinciding with the z axis) is energetically most favorable for the following reason: the total energy stored per unit length is proportional to b^2 (**b** is the Burgers vector).[1,2,4] The (111) planes (one of the (111) planes contains the z axis) are most densely packed and contain the smallest possible Burgers vector $\mathbf{b}=a\mathbf{u}_x/2^{1/2}$ that accordingly minimizes the total energy stored per unit length. However, since this **b** contains two atomic planes, it can be further divided into two partial Burgers vectors $\mathbf{b}_1$ and $\mathbf{b}_2$:

$$\mathbf{b}=\mathbf{b}_1+\mathbf{b}_2=(a\mathbf{u}_x/2^{1/2}-a\mathbf{u}_y/6^{1/2})/2+(a\mathbf{u}_x/2^{1/2}+a\mathbf{u}_y/6^{1/2})/2. \tag{11}$$

Since $b^2>b_1^2+b_2^2$ the [112] edge dislocation has a tendency to separate into two partial dislocations. This tendency is also seen in the MD simulations.

The initial geometry of the perfect [112] edge dislocation was prepared according to the Cotterill-Doyama recipe.[4] First, the yz-half-plane II ($y<0$) of atoms as well as the parallel half-plane I to the left (see Fig. 2) were removed. Secondly, the parallel half-plane III on the right-hand side was moved by $-\mathbf{b}/2$ to coincide with the yz plane. Thirdly, the atoms for $x>0$ were displaced according to the elastic-continuum theory[1,2] and the atoms for $x<0$ were displaced symmetrically with respect to the yz plane. (However, the atoms closest to the z axis were displaced only by half of the displacements to prevent the coincidences with the yz-plane atoms.)

Figure 3 shows a top view of the left part and the center of the initial symmetric configuration for copper. We use periodic boundaries with the period of $L_z=1.5\times 6^{1/2}a$ containing 18 atomic planes in the [112] direction (z axis) perpendicular to the plane of Fig. 3 ($a=3.615$ Å for copper). The initial configuration for gold is similar to that for copper.

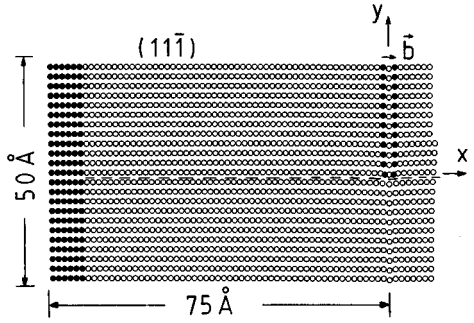

FIG. 3. The xy projection (top view) of the initial configuration of copper. The configuration is symmetric with respect to the yz plane. Filled circles represent fixed atoms of the boundary layer and open circles movable atoms except that the two chains of filled circles represent movable atoms of the two extra atomic half-planes. **b** is the Burgers vector. The dashed line represents the slip plane. For further information see the caption of Fig. 2.

The x and y dimensions equal 170 and 55 Å, respectively. These numbers are obtained by scaling approximately the dimensions of copper by the ratio $a_{\mathrm{Au}}/a_{\mathrm{Cu}}=4.078$ Å/3.615 Å$\approx$1.128. The two chains of filled circles in Fig. 3 represent the two atomic half-planes forming the initial edge dislocation. Both far ends of the system are held immobile (the filled circles at the left end in Fig. 3). Two types of (111) boundaries are used: (i) free (111) boundaries as shown in Fig. 3 and (ii) the four outermost (111) planes on both sides held immobile. Both types of boundaries are used in calculating the structure of the DR and the structures and formation energies of point defects in the DR in order to check the possible effects of the (111) boundaries on these quantities. However, only the immobile (111) boundaries are used in migration studies at high temperatures where the free (111) boundaries could disorder significantly and even melt. To remove artificial thermal stresses the whole system including the immobile boundaries is scaled at each temperature according to the thermal expansion calculated by Holender for the ATVF model[23] and constant-NTV MD is then used to equilibrate the system properly at the corresponding temperature.

IV. INTERACTIONS AND STRUCTURES

A. Partial dislocations

Two methods as well as the free and immobile $(\bar{1}\bar{1}\bar{1})$ boundaries were used in calculating the interaction energy between the partial dislocations and their relaxed structures. In the *quasidynamic* method a large positive constant friction coefficient $\xi=10^{15}$ s^{-1} is used in Eq. (1) to damp out kinetic energy. Convergence is accelerated by using the following individual damping method:[24] when $\mathbf{v}_i\cdot d\mathbf{v}_i/dt<0$, $\mathbf{v}_i$ is set to zero. The quasidynamic method should give the closest local minimum of the total potential energy $\mathscr{V}$ from the initial configuration of Fig. 3.

As the second method we used the *heating-cooling cycle*. In this method temperature is first increased and then decreased stepwise. At each step the whole system (including the immobile boundaries) is scaled according to the calculated thermal expansion of the ATVF model[23] and constant-

TABLE I. Calculations for the relaxed structures of the partial dislocations. t_A and t_M are the total times used in the quasidynamics and the combined microcanonical-quasidynamics approach, respectively. $T_{\max}$ and t_B are the maximum temperature and the total time, respectively, used in the heating-cooling cycle $0K \rightleftarrows T_{\max}$. d_A, d_M, d_B, and $d_{\rm el}$ are the separation distances of the partial dislocations obtained using quasidynamics, the combined microcanonical-quasidynamics approach, the heating-cooling cycle, and the elastic-continuum theory, respectively.

Metal	$(11\bar{1})$ boundaries	t_A (ps)	d_A (Å)	t_M (ps)	d_M (Å)	$T_{\max}$ (K)	t_B (ps)	d_B (Å)	$d_{\rm el}$ (Å)
Copper	Free	584	31	1150	40	500	525	77	42
	Immobile					1000	450	55	
Gold	Free	511	24			500	525	88	43
	Immobile					1000	1350	66	

NTV MD is used to equilibrate the system properly at each temperature. The heating-cooling cycle should give the global minimum of $\mathscr{V}$. Our calculations are summarized in Table I.

We discuss first the behavior of $\mathscr{V}$ of the copper system of Fig. 3 [free (111) boundaries, 8007 atoms] as a function of the separation distance of the partial dislocations d. $\mathscr{V}$ consists of[1,2,4] (i) the linearly increasing attractive stacking-fault energy, (ii) the repulsive interaction energy falling asymptotically to zero, and (iii) the periodic Peierls-Nabarro energy. The calculated $\mathscr{V}(d)$ is shown in Fig. 4. The set of points ending at A is calculated with the quasidynamic method. Point A is the closest local minimum of $\mathscr{V}$ from the initial configuration of Fig. 3 (see the upper inset of Fig. 4). Point M is obtained by using microcanonical MD [$\xi=0$ in Eq. (1)] up to the separation distance where the absolute minimum of $\mathscr{V}$ is expected to lie and then by using the quasidynamic method to relax the system. Point B results from a heating-cooling cycle. The heating to 500 K increases the separation of the partial dislocations up to 85 Å and during the subsequent cooling the system is trapped in a local Peierls-Nabarro minimum at a large separation. According to our experience it seems to be very difficult to obtain the absolute minimum for a large system (8007 atoms here) in a reasonable computing time using this straightforward method. The energies of points A, B, and M result all from well-converged calculations. The solid curve in Fig. 4 is the lower envelope function of the calculated $\mathscr{V}$ including the contributions (i) and (ii). The dashed line is the elastic-continuum potential energy expression[4]

$$\mathscr{V}_{\rm el}=\mathscr{V}_0-L_z\frac{\mu a^2}{48\pi}\left(\frac{2+\nu}{1-\nu}\right)\ln\left(\frac{d}{\text{Å}}\right)+L_z\gamma d \qquad (12)$$

fitted to the calculated points M and B. In Eq. (12) $\mathscr{V}_0$ is a constant determined by the fitting, $L_z=1.5\times 6^{1/2}a=13.3$ Å is the z dimension of the MD cell, $\mu=4.85\times10^{10}$ kg m^{-1} s^{-2} (Ref. 1), ν is Poisson's ratio$=0.35$ (Ref. 1), and γ is the stacking fault energy$=36$ mJ/m^2 (Ref. 15). The fit is very successful: $\mathscr{V}$ and $\mathscr{V}_{\rm el}$ differ at points M and B only by 5.2 meV (or 0.4 meV/Å).

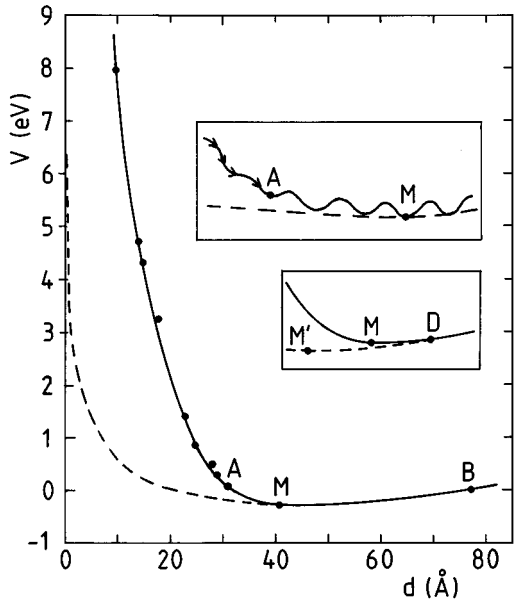

FIG. 4. The calculated behavior of the total potential energy $\mathscr{V}$ as a function of the separation distance of the partial dislocations d for copper. The free (111) boundaries are used. The set of points ending at A is calculated with the quasidynamic method. Point M is obtained with the combined microcanonical-quasidynamics approach. Point B results from a heating-cooling cycle. The solid curve is the lower envelope function of $\mathscr{V}$. The dashed line is the elastic-continuum approximation $\mathscr{V}_{\rm el}$ of Eq. (12). The upper inset shows schematically $\mathscr{V}$ around points A and M. The lower inset shows schematically the neighborhood of the minimum M for a large stacking fault energy (M' denotes the minimum of $\mathscr{V}_{\rm el}$ and D the point where the lower envelope function of $\mathscr{V}$ and $\mathscr{V}_{\rm el}$ start to deviate). $\mathscr{V}$ is calculated for the 8007 atoms of the MD cell having the z dimension $L_z=13.3$ Å.

Our calculated result in Fig. 4 is consistent with the common picture that the elastic-continuum theory describes well the interaction of two partial dislocations for large distances (the Peierls-Nabarro variation is not taken into account in this comparison). The atomic cores of the partial dislocations are seen to start to interact repulsively at the absolute minimum M where the calculated lower envelope function starts to depart from $\mathscr{V}_{\rm el}$. This indicates a negligible core overlap at the equilibrium separation distance d_M and a core extent of about $d_M/2\approx20$ Å.

The stacking fault energy of the ATVF model $\gamma=36$ mJ/m^2 represents a small value in the experimental range 30–80 mJ/m^2 (see Refs. 4, 6, 7, 10, 11, and 15). Since $d_{M'}$ of the minimum M' of $\mathscr{V}_{\rm el}$ is proportional to γ^{-1} [Eq. (12)] we may expect that for a large γ $d_{M'}<d_M$ as shown in the lower inset of Fig. 4. In this case the atomic cores overlap ($d_D>d_M$). Häkkinen *et al.*[6] using the many-atom effective-medium theory (EMT) with $\gamma=79$ mJ/m^2 found an equilib-

rium separation distance of 27 Å and a relatively small core overlap with a core extent of about 16 Å (the Burgers vector distribution in the middle of the fault ribbon is about 13% of the maximum value at $T=0$ K). Their equilibrium separation distance was obtained by starting from a configuration similar to that in Fig. 3 and by removing the kinetic energy after each 0.03 ps (=10 MD time steps). Their method resembles the quasidynamic method. Since their separation distance of 27 Å is less than their elastic-continuum distance $d_{M'}=29$ Å their calculation may have gotten trapped in a local Peierls-Nabarro minimum before M (see the range $A-M$ in the upper inset of Fig. 4). Thus the real equilibrium separation distance would possibly be larger, which would decrease the core overlap. Huang *et al.*[7] using a long-range interaction potential in the PPA with $\gamma=73$ mJ/m^2 found a separation distance of 23 Å and a significant core overlap with a core extent of about 17 Å (the Burgers vector distribution in the middle of the fault ribbon is about 33% of the maximum value at $T=107$ K). Since the approximate core extents in the above calculations are not very different the main factor determining the core overlap is the equilibrium separation distance expected to be proportional to γ^{-1}. Consistently, our ATVF calculation with a small γ of 36 mJ/m^2 gives a large d_M of 40 Å whereas the EMT calculation[6] and the calculation of Ref. 7 with a large γ (79 and 73 mJ/m^2, respectively) give a smaller d_M (27 and 23 Å, respectively). However, the relative magnitude of the smaller distances d_M appears to depart from the expected trend. This may be due to the fact that calculated values of d_M can depend sensitively on the details of the interaction model[25–27] and to some extent on the calculational method and/or boundaries used (cf. Table I).

The calculated $\mathscr{T}(d)$ for gold in the case of free boundaries behaves very similarly to $\mathscr{T}(d)$ for copper in Fig. 4 [$\mathscr{T}_{\rm el}(d)$ for gold (Eq. (12)] was calculated by using the following parameters: $a=4.078$ Å, $\mu=2.78\times10^{10}$ kg m^{-1} s^{-2} (Ref. 1), $\nu=0.42$ (Ref. 1), and $\gamma=32$ mJ/m^2 (Ref. 15). We estimate for gold an equilibrium separation distance of about 42 Å and a core extent of about 21 Å indicating a negligible core overlap also in this case. We also notice that in the case of the immobile (111) boundaries the heating-cooling cycles result in somewhat smaller separation distances than in the case of the free (111) boundaries for both metals (Table I) which can be due to the fact that the immobile (111) boundaries—adjusted originally for the perfect dislocation—may damp the separation to some extent. We finally notice that our calculated separation distances for both metals have a tendency to increase with increasing temperature for both (111) boundaries which differs from the constant distance found in Ref. 7. In addition to the damping effect of the immobile (111) boundaries mentioned above this difference must be due to differences in the potentials. The small $\gamma=36$ mJ/m^2 of the ATVF model makes $\mathscr{T}(d)$ of copper relatively flat for $d>d_M$ (see Fig. 4) which allows an easy separation when temperature is increased whereas the large $\gamma=73$ mJ/m^2 in Ref. 7 should make $\mathscr{T}(d)$ more steeply rising for $d>d_M$ which has a tendency to prevent the separation. (Moreover, the separation may depend sensitively on the details of the interaction model.[25–27])

As to the atomic structures around the partial dislocations we find *virtually identical* structures both for copper and gold in all cases listed in Table I indicating that the structures

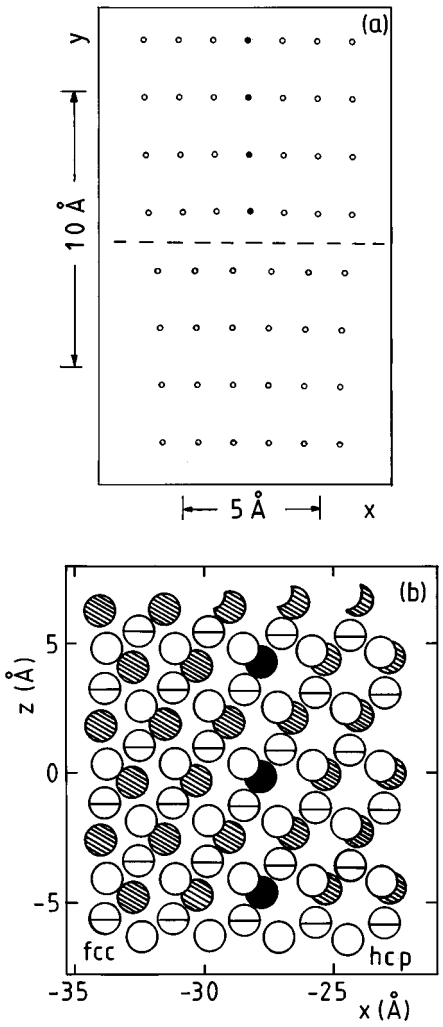

FIG. 5. The structure of the partial dislocation of copper after the heating-cooling cycle (point B). (a) The xy projection (top view) of the left partial dislocation. The filled circles represent the atoms of the atomic half-plane of the partial dislocation. The dashed line represents the slip plane. (b) The xz projection (side view) of the atoms of the plane including the edges of the partial dislocations and of the two adjacent planes on the other side of the slip plane. Only one period of the atoms in the z direction is shown. The edge atoms of the partial dislocation are denoted by filled circles and the other atoms in the same (111) plane are denoted by shaded circles. The atoms of the adjacent plane are denoted by circles with a bar and the atoms of the next plane towards the negative y axis by open circles.

are neither very sensitive to the $(11\bar{1})$ boundaries used nor to the size of the separation distance. Figure 5(a) shows a top view of the atomic structure around the left partial dislocation in copper. An examination reveals here a distinct local enhancement of the distance between the (111) atomic planes at the slip plane compared with the corresponding distance of $a/3^{1/2}$ in the crystal. A similar enhancement is also seen in gold and in Ref. 6 in copper. Figure 5(b) shows a side view of the atoms in the (111) atomic plane including the edge of the partial dislocation and in the two (111) atomic planes towards the negative y axis at the left partial dislocation. The transition strip from the fcc stacking outside the DR to the hcp stacking fault is approximately 34 Å wide [see Fig. 5(b)]

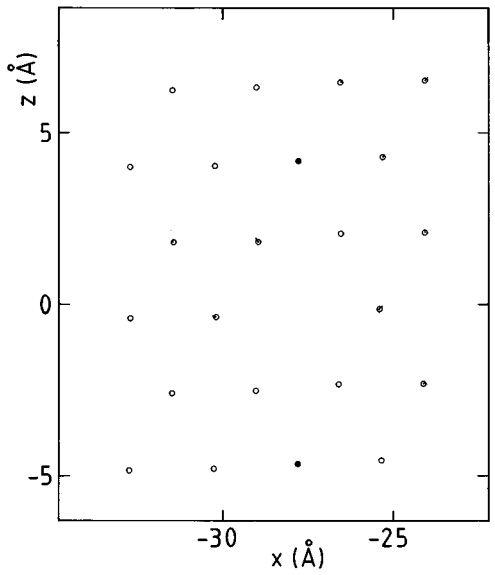

FIG. 6. The structure of a vacancy on the edge of the left partial dislocation of copper (side view). The atoms of the (111) plane containing the edges of the partial dislocations are shown. The filled circles represent the edge atoms of the partial dislocation. Small bars show the relaxations of the atoms.

and the core extent is approximately 17 Å. About the same values are obtained also for gold. However, these values are not very accurate because it is difficult to find exact geometric criteria for the width of the transition strip.

B. Vacancies and interstitials near partial dislocations

The atomic structures and formation energies of a vacancy and an interstitial at the edge of a partial dislocation were studied using both the free and immobile (111) boundaries. The calculations were performed at point *B* (Fig. 4 and Table I) because it is best compatible with the self-diffusion studies of Sec. V and because the results can be expected to depend very little on the separation distance of the partial dislocations anyway. The relaxed structures were obtained by performing 10 000 constant-*NTV* MD time steps at 1 K ($\delta t = 2.5$ fs).[28] The obtained structures are found to be *virtually independent of the type of the* (111) *boundaries* used and similar for both metals. Figure 6 shows the side view of the obtained configuration of a vacancy in the (111) plane at the left partial dislocation in copper. The relaxed vacancy has clearly the form of a distorted hexagon with the (expected) small inward relaxations of the surrounding atoms indicated by the bars in the figure. Häkkinen *et al.*[6] also found a corresponding distorted hexagon in copper. Notice that the main distortion is already present in the starting configuration [Fig. 5(b)]. The distortion is a direct consequence of the fact that the stacking fault constrains the atoms [the shaded circles in Fig. 5(b)] to shift upwards when the fault region is approached.

Figure 7(a) shows a top view of the configuration of an interstitial (the filled square) at the left partial dislocation in copper. The relaxed interstitial position is found in the (111) atomic plane in front of the partial dislocation. The original position of the added atom is indicated by an open square. Although the final interstitial atom is the same as the added

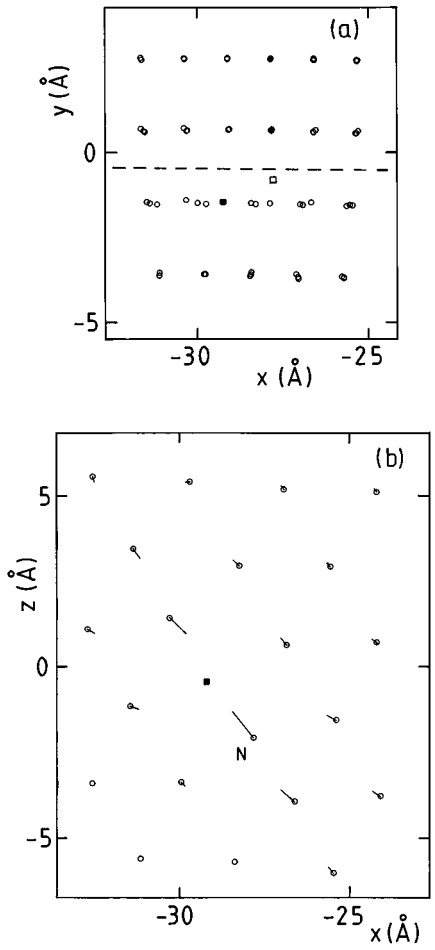

FIG. 7. The structure of an interstitial at the left partial dislocation in copper. The filled square represents the interstitial atom. The open square shows the original position of the added atom. (a) The *xy* projection (top view). The filled circles represent the atoms of the atomic half-plane of the partial dislocation. The dashed line represents the glide plane. (b) The *xz* projection (side view) of the atoms in the $(11\bar{1})$ plane containing the interstitial atom. The bars show the relaxations of the atoms. *N* denotes the nearest atom to the interstitial.

atom the role of the interstitial was temporarily transferred to another atom in the same (111) atomic plane during the transient. Figure 7(b) shows a side view of the (111) plane. The obtained interstitial is a crowdion[29] along the ⟨110⟩ line (the $-\mathbf{u}_x+3^{1/2}\mathbf{u}_z$ direction in Fig. 2). The distance between the interstitial and the nearest atom *N* equals 2.10 Å. The interatomic distances then grow alternatingly as 2.15; 2.23, 2.27; 2.38, and 2.42 Å along the ⟨110⟩ line. These distances are less than the interatomic distance $a/2^{1/2}=2.56$ Å in an ideal (111) plane showing that the distorted region reaches beyond the third nearest neighbors along the ⟨110⟩ line. There is also another (though here less natural) way of viewing the interstitial and the *N* atom as a ⟨110⟩ split interstitial.[29] The obtained length of the split interstitial is 2.1 Å and the obtained angle between the split interstitial and the edge of the [112] partial dislocation (*z* direction) is 40°. These numbers agree closely with the findings by Huang *et al.*[11] Notice also that the obtained ⟨110⟩ crowdion structure differs from the ⟨100⟩ dumbbell structure found in the bulk.[15] In the case of gold

TABLE II. Point defect formation energies. E_f^v, E_{fb}^v, E_f^i, and E_{fb}^i denote the formation energies for a vacancy on the edge of a partial dislocation, a vacancy in the bulk, an interstitial at the edge of a partial dislocation, and an interstitial in the bulk, respectively. PPA, PSP, EMT, and ATVF denote the pair-potential approximation, pseudopotential, effective-medium-theory, and Ackland-Tichy-Vitek-Finnis, respectively. The numbers of the present work without the parentheses are calculated using the immobile (111) boundaries and those in the parentheses using the free (111) boundaries.

Authors	Model	Metal	E_f^v (eV)	E_{fb}^v (eV)	E_f^i (eV)	E_{fb}^i (eV)
Fidelman and Zhuravlev[a]	PPA	Cu	0.69	0.87		
		Au	0.60	0.74		
Huang *et al.*,[b,c] Lam *et al.*[d]	PPA[b,c] PSP[d]	Cu	1.05,[b],1.15[c]	1.42[d]	1.75,[b]1.82[c]	2.61[d]
Häkkinen *et al.*[e]	EMT	Cu	1.33	1.47		
Present work, Ackland *et al.*[f]	ATVF	Cu	0.97 (0.96)	1.191[f]	1.81 (1.79)	3.62[f]
		Au	0.85 (0.85)	0.962[f]	1.93 (2.03)	4.35[f]
Experiments[g,h]		Cu		0.95–1.31[g]		2.2[h]
		Au		0.82–1.0[g]		

[a]Reference 5.
[b]Reference 11.
[c]Reference 10.
[d]Reference 30.
[e]Reference 6.
[f]Reference 15.
[g]References 31,32.
[h]Reference 33.

the transient was more complex including several transfers of the role of the interstitial to different atoms and, in fact, the final interstitial atom is not the same as the added atom. The obtained alternatingly growing interatomic distances of the ⟨110⟩ crowdion for gold are 2.48, 2.51; 2.59, 2.63; 2.73, and 2.78 Å [the interatomic distance $a/2^{1/2}=2.88$ Å in an ideal (111) plane]. Thus the distorted region reaches beyond the third nearest neighbors along the ⟨110⟩ line also in this case. Notice that the obtained ⟨110⟩ crowdion structure differs from the octahedral structure found in the bulk.[15]

The formation energies E_f, calculated from the equation

$$E_f=\mathscr{V}(N\mp 1)-(N\mp 1)\mathscr{V}(N)/N \tag{13}$$

are summarized in Table II together with those calculated recently by other authors and with the experimental formation energies.[5,6,10,11,15,30–33] We find that the calculated formation energies depend *very little on the type of the* (111) *boundaries* used [compare the values obtained with the immobile (111) boundaries with those obtained with the free (111) boundaries given in the parentheses]. All the calculated formation energies in the bulk show a reasonable agreement with the experimental values.[34] All the calculations show that the formation energies are lower at the edge of a partial dislocation than in the bulk.[35] The formation energy of an interstitial is lowered significantly more than that of a vacancy opening the interesting possibility that self-diffusion in the DR could be mainly due to interstitials instead of vacancies (the vacancy mechanism is the main mechanism in the bulk).

V. SELF-DIFFUSION

A. Migration of single defects

The migration of vacancies and interstitials is calculated at relatively high temperatures using long MD simulations of the order of 1.5 ns. Due to the limitations of available computing time we chose to study migration only for gold. For the ATVF model of gold the melting temperature $T_m=1475$ K, compared with the experimental value of $T_m=1336$ K.[23] We performed constant-NTV MD simulations for migration in the temperature range 1000–1400 K using the immobile (111) boundaries. In order to avoid disorder in the DR we heated the gold system rather slowly by increasing temperature T by increments of 50 K and scaled the whole system including the immobile boundaries at each T according to the calculated thermal expansion of the ATVF model.[23] Up to 10 000 time steps of 2.5 fs were used to equilibrate the system at each temperature. Above $T=1000$ K we used a smaller increment of 25 K. Although the instantaneous atomic arrangements above $T=1000$ K are quite irregular we could nevertheless locate the temporal positions of the partial dislocations.

Our first approach was to use the coordination density method (see Sec. II B) to monitor the migration of a single vacancy or interstitial. At each temperature a vacancy was created on the edge of the (left) partial dislocation and an interstitial was created by adding one atom in front of the edge of the partial dislocation to a center of mass defined by one atom on the edge and the two nearest neighbor atoms in the adjacent (111) atomic plane. The results of these calculations are summarized in Table III.

The migration of the vacancy occurs as relatively sudden jumps with a frequency of ~0.1 THz at temperatures 1300 and 1400 K. However, in about 60 ps the value of b_t [Eq. (8)] at the vacancy increased permanently to values charac-

TABLE III. Migration of single defects in the dislocation region using the coordination density method. Δt denotes the time one can follow the defect. T denotes the temperature.

Defect	T (K)	Events	Δt (ps)
Vacancy	1000	0 jumps	
	1300	4 jumps	61
	1400	6 jumps	66
Interstitial	1000	1 role transfer	0.075
	1300	2 role transfers	0.130
	1400	4 role transfers	0.100

teristic for empty regions in a regular crystal and one is not able to any more identify the single vacancy inside the vacancy sphere. (The value of b_t increased also during some of the jumps temporarily to values characteristic for empty regions in a crystal but b_t was again dropped back to small values after the jump was completed.) Although the data obtained for the migration of a single vacancy is not statistically sufficient one can derive a rough estimate for the vacancy migration energy E_m^v. By assuming that the jump frequency ν obeys the Arrhenius-type relation

$$\nu = Ae^{-E_m^v/(k_B T)}, \tag{14}$$

where A is a proportionality constant and using the calculated values $\nu(1300\ \mathrm{K})=4/61$ THz and $\nu(1400\ \mathrm{K})=6/66$ THz we obtain for E_m^v the value ~ 0.5 eV.

The migration of the interstitial (see Table III) occurs as frequent ($\sim$13–40 THz) role transfers (i.e., the role of the interstitial is transferred from one atom to another neighbor atom) on the side of tension. However, these frequent events could be followed only for very short times of roughly 100 fs after which b_t dropped permanently to values characteristic for atoms in a regular crystal. (Occasional drops of b_t to values characteristic for a regular crystal were also observed during the transfer processes.) Thus the identity of the interstitial is lost at high temperatures very soon. Similar difficulties to follow self-defects at high temperatures were also met in Ref. 36. A rough estimate using the calculated numbers of transfers in Table III and Eq. (14) (with E_m^v replaced by E_m^i) gives for the interstitial migration energy E_m^i the value ~ 0.2 eV.

B. Induced mass transport

To circumvent the problems in Sec. V A we chose—parallel to Refs. 37 and 38—as our second approach to calculate directly the net mass transport induced by one vacancy or one interstitial using constant-NTV MD. To improve statistics one vacancy (interstitial) is created on (in front of) the edge of each partial dislocation at each temperature. The diffusion constant induced by one vacancy is then calculated from the equation

$$D_v = \frac{1}{2}\,[D(N-2) - D(N)] \tag{15}$$

and that induced by one interstitial from the equation

$$D_i = \frac{1}{2}\,[D(N+2) - D(N)], \tag{16}$$

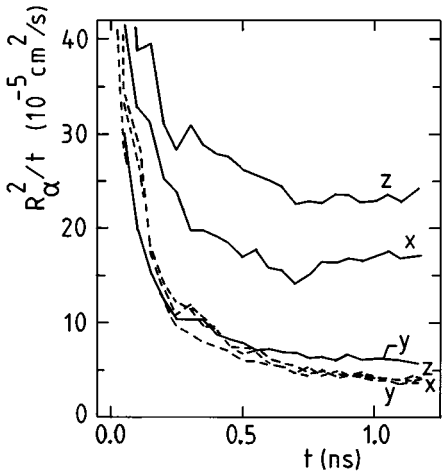

FIG. 8. The convergence of $(1/t)R_\alpha^2=(1/t)\Sigma_i[r_{i\alpha}(t)-r_{i\alpha}(0)]^2$ ($\alpha=x,y,z$) for gold at $T=1300$ K. The solid and dashed lines are the results for $N+2$ and $N-2$ movable atoms ($N=4683$), respectively.

where the diffusion constant D is given in Eq. (9). Thus we assume here that the mass transports induced at both partial dislocations remain sufficiently separate to allow the use of Eqs. (15) and (16).

The constant-NTV MD simulations of $\approx$1.5 ns each are performed at the temperatures 1150, 1300, and 1400 K for $D(N+2)$, $D(N-2)$, and $D(N)$. Figure 8 shows the convergence of the quantities R_α^2/t [$\alpha=x,y,z$; see Eq. (10)] for the $N+2$ and $N-2$ atom systems (solid and dashed lines, respectively) at $T=1300$ K. R_α^2/t for the N atom system (not shown in Fig. 8) are similar to and lie slightly below those of the $N-2$ atom system. The convergence appears to be quite satisfactory and—because only differences are needed in Eqs. (15) and (16)—sufficient for our purposes. A convergence of the same type was also obtained at $T=1150$ and 1400 K.

The calculated diffusion constants induced by one vacancy or one interstitial are summarized in Table IV. The self-diffusion induced by one interstitial is about 3–16 times as large as the self-diffusion induced by one vacancy. The value of D_i at 1400 K is anomalously low. The reason for this behavior is not clear to us. One possibility is that the mass transport induced by the interstitial in the DR penetrates at 1400 K to the regions of low migration in the bulk (this behavior was found in Ref. 11 for vacancies).

A least-squares fit to the Arrhenius law $D_v \propto \exp[-E_m^v/(k_B T)]$ gives for the migration energy for a vacancy E_m^v a value of 0.75 eV. Since the value of D_i at 1400

TABLE IV. The calculated diffusion constants induced by one vacancy or one interstitial in gold. D_{vx}, D_{vy}, D_{vz} and D_{ix}, D_{iy}, D_{iz} denote the Cartesian components (for the coordinate axes see Figs. 2 and 5) of the diffusion constants induced by one vacancy and one interstitial, respectively. The total induced diffusion constants D_v and D_i are sums of the Cartesian components. All diffusion constants are given in units 10^{-6} cm^2/s

T (K)	D_{vx}	D_{vy}	D_{vz}	D_v	D_{ix}	D_{iy}	D_{iz}	D_i
1150	1.2	0.5	1.2	2.8	17.3	0.7	26.2	44.3
1300	2.3	2.6	2.6	7.5	23.9	6.1	35.6	65.6
1400	4.0	3.7	4.0	11.7	11.5	7.3	13.4	32.1

TABLE V. Migration energies. E^v_m, E^v_{mb}, E^i_m, and E^i_{mb} denote the migration energies for a vacancy near the partial dislocation, a vacancy in the bulk, an interstitial near the partial dislocation, and an interstitial in the bulk, respectively. PPA, PSP, and ATVF denote the pair-potential approximation, pseudopotential, and Ackland-Tichy-Vitek-Finnis, respectively.

Authors	Model	Metal	E^v_m (eV)	E^v_{mb} (eV)	E^i_m (eV)	E^i_{mb} (eV)
Fidelman and Zhuravlev[a]	PPA	Cu	0.74–0.81	0.98		
		Au	0.55–0.59	0.72		
Huang *et al.*,[b,c] Lam *et al.*[d]	PPA,[b,c] PSP[d]	Cu	0.67,[b] 0.77[c]	0.82[d]	0.075,[b] 0.13[c]	0.11[d]
		Au		0.71[d]		0.11[d]
Present work	ATVF	Au	0.75		$\lesssim$0.1	

[a]Reference 5.
[b]Reference 11.
[c]Reference 10.
[d]Reference 30.

K in Table IV is anomalously low a straightforward fit to the Arrhenius law would give a negative and thus an unphysical value for the migration energy for an interstitial E^i_m. However, the data for an interstitial in Table IV clearly indicates that E^i_m must be close to zero. We therefore estimate a value $\lesssim$0.1 eV for E^i_m. Our results are summarized in Table V together with the migration energies calculated by other authors.[5,10,11,30] Table V displays the following general features. The migration energies for an interstitial are significantly ($\sim$0.6–0.7 eV) smaller than those for a vacancy, both in the DR and in the bulk. The migration energies for a vacancy in the DR are slightly smaller than those in the bulk. The limited data for the migration energies for an interstitial show only that they have about the same size in the DR as in the bulk. We also notice that our rough estimates above $E^v_m \sim 0.5$ eV and $E^i_m \sim 0.2$ eV agree reasonably well with our respective values 0.75 and $\lesssim$0.1 eV given in Table V.

The activation energies (sums of the formation and migration energies from Tables II and V) are summarized in Table VI.[5,10–12,30] As expected, the activation energies for the self-diffusion in the DR are less than in the bulk. Our calculated activation energy for the vacancy mechanism in the DR in gold is at least 0.33 eV less than for the corresponding interstitial mechanism indicating that the former is the main mechanism in the DR. Thus the interstitial formation energy does not decrease sufficiently from the value in the bulk to the value at the edge of the partial dislocation to make the interstitial mechanism competitive with the vacancy mechanism in gold.

The estimates for the activation energies in the DR in copper are obtained as follows. The calculation by Fidelman and Zhuravlev[5] indicates that E^v_m for copper is about 0.2 eV larger than for gold (see Table V). We thus estimate using $E^v_m = 0.75$ eV for gold that E^v_m for copper is 0.9–1.0 eV. Summing this with $E^v_f = 0.97$ eV (Table II) we get the estimate $E^v_D \approx 1.9$–2.0 eV given in Table VI. Table V indicates that a reasonable value for E^i_m for copper could be 0.1–0.2 eV. Summing this with $E^i_f = 1.81$ eV (Table II) we get the estimate $E^i_D \approx 1.9$–2.0 eV given in Table VI. Thus in the DR of copper $E^i_D \approx E^v_D$ and the interstitial mechanism would become a real competitive mechanism for the vacancy mechanism which is in line with the results by Huang *et al.*[10,11]

We next consider the sizes of our calculated diffusion constants. By using Eq. (9) we obtain for the reference system including the two partial dislocations but no vacancies or interstitials the diffusion constant $D_r(1400\ \mathrm{K}) = 9.8\times10^{-6}$ cm^2/s. This value is consistently somewhat smaller than the diffusion constant $D = 37.5\times10^{-6}$ cm^2/s calculated by Mei and Davenport for liquid gold close to T_m using the embedded-atom model.[39] De Lorenzi and Ercolessi have calculated the diffusion constant induced by one vacancy in the bulk for gold using the glue model.[38] At T_m they obtain the value $D_{vb} \approx 2.3\times10^{-8}$ cm^2/s that is consistently smaller than our calculated value in the DR: $D_v(1400\ \mathrm{K}) = 11.7\times10^{-6}$ cm^2/s (Table IV).

The geometry of the DR is clearly reflected in the cartesian components of the diffusion constants D_i induced by an interstitial (see Table IV). At all temperatures D_{iz} along the

TABLE VI. Activation energies. E^v_D, E^v_{Db}, E^i_D, and E^i_{Db} denote the activation energies for a vacancy mechanism near the partial dislocation, a vacancy mechanism in the bulk, an interstitial mechanism near the partial dislocation, and an interstitial mechanism in the bulk, respectively. PPA, PSP, and ATVF denote the pair-potential approximation, pseudopotential, and Ackland-Tichy-Vitek-Finnis, respectively. The numbers in parentheses are estimates (see the text).

Authors	Model	Metal	E^v_D (eV)	E^v_{Db} (eV)	E^i_D (eV)	E^i_{Db} (eV)
Fidelman and Zhuravlev[a]	PPA	Cu	1.43–1.50	1.85		
		Au	1.15–1.19	1.46		
Huang *et al.*,[b,c] Lam *et al.*[d]	PPA,[b,c] PSP[d]	Cu	1.72,[b] 1.92[c]	2.24[d]	1.82,[b]1.95[c]	2.72[d]
		Au		3.46[d]		3.92[d]
Present work	ATVF	Cu	(1.9–2.0)		(1.9–2.0)	
		Au	1.6		1.93–$\sim$2.0	
Experiment		Cu	1.53[e]			

[a]Reference 5.
[b]Reference 11.
[c]Reference 10.
[d]Reference 30.
[e]Reference 12.

partial dislocations are the largest, D_{ix} along the stacking fault ribbon somewhat smaller, and D_{iy} perpendicular to the stacking fault ribbon by far the smallest. The components of the diffusion constants D_v induced by a vacancy show similar tendencies though much more weakly: D_{vx} and D_{vz} are approximately equal and D_{vy} grows to the same size as D_{vx} and D_{vz} at higher temperatures (1300 and 1400 K). The MD calculations for copper by Huang *et al.*[11] resulted in the same type of behavior between the components of the induced diffusion constants. Our results show that self-diffusion in the DR in gold is not simply mass-transport along the edges of the partial dislocations (in which case the x and y components would be practically vanishing). Instead, since the vacancy mechanism is dominant, self-diffusion has equally strong x and z components in the DR, the y component growing at higher temperatures. On the other hand, if vacancies and interstitials are created nonthermally (e.g., by particle irradiation) it is clear that the subsequent migration in the DR is dominated by interstitials (Table IV). Self-diffusion shows in this case a more profound two dimensionality in the xz-stacking-fault plane, the z component along the edges of the partial dislocations being the largest component (Table IV). The spread of self-diffusion into the whole DR was also observed in the MD study by Huang *et al.* for copper.[10,11] One might hence think that also more generally when a stacking fault ribbon opens, self-diffusion has a tendency to spread into this region of lower symmetry. This two-dimensional behavior in turn has a tendency to reduce the component along the edge of the dislocation which would dominate alone in the case of a single dislocation. Thus this mechanism naturally explains why there is the general tendency in metals that observed self-diffusion is weaker along partial dislocation pairs than along perfect dislocations.

VI. CONCLUSIONS

We draw the following conclusions from our MD studies of the partial dislocations in copper and gold using the ATVF model.

(i) The calculated interaction energy between the partial dislocations in copper is found to agree accurately with the elastic-continuum energy beyond and at the equilibrium separation distance whereas the former energy grows much more strongly at smaller separation distances due to the increased core repulsion. This behavior indicates a small core overlap at the equilibrium. Similar results are also obtained for gold. The distance between the (111) atomic planes is found to show a distinct increase at the slip plane in front of the edges of the partial dislocations.

(ii) We find that a vacancy at the edge of a partial dislocation has a form of a distorted hexagon in the (111) atomic plane for both metals. Since the relaxations of the atoms for the removal of an atom are small the distortion is a direct consequence of the existence of a stacking fault ribbon. We find that an interstitial forms a long $\langle 110 \rangle$ crowdion in the (111) atomic plane in front of the edge of a partial dislocation for both metals. We find that the calculated formation energy for a vacancy at the edge of a partial dislocation decreases only by about 0.2 (0.1) eV compared to the bulk value whereas that for an interstitial near the edge of a partial dislocation decreases by 1.9 (2.4) eV compared to the bulk value in copper (gold).

(iii) Self-diffusion was studied in the region of the partial dislocation pair in gold. We find, as expected, that the migration rate induced by an interstitial is significantly larger than that induced by a vacancy. Thus if both interstitials and vacancies would be available, the interstitial mechanism would be the dominant diffusion mechanism. However, the formation energy of an interstitial at the edge of a partial dislocation is about 1.1 eV larger than that of a vacancy. This makes the activation energy for thermal self-diffusion with the vacancy mechanism at least 0.33 eV smaller than that for the interstitial mechanism in the region of the partial dislocation pair. We estimate that the corresponding activation energies in copper would be approximately equal.

(iv) The self-diffusion induced by a vacancy in the region of the partial dislocation pair in gold is found to have equally strong components along the [112] edges of the partial dislocations and the stacking fault ribbon. (The component perpendicular to the fault ribbon is found to be smaller but grows to the same size at higher temperatures.) Thus, when a stacking fault ribbon is opened, self-diffusion spreads into this region of lower symmetry reducing the component along the edge of the partial dislocation. This component would dominate alone in the case of a single dislocation. We believe that this mechanism can naturally explain why self-diffusion in metals has a tendency to be weaker along partial dislocation pairs than along perfect dislocations.

APPENDIX

Equations (1) and (2) are solved by generalizing the standard velocity-Verlet algorithm[3,21] as follows. The full step velocities are calculated from the equation

$$\mathbf{v}_i(t+\delta t)=\mathbf{v}_i\left(t+\frac{1}{2}\,\delta t\right)+\frac{1}{2}\,\delta t\left[\frac{\mathbf{f}_i(t+\delta t)}{m}-\xi(t+\delta t)\mathbf{v}_i(t+\delta t)\right] \tag{A1}$$

and the full step friction coefficient using Simpson's formula

$$\xi(t+\delta t)=\xi(t)+\frac{\delta t}{6}\left[\dot{\xi}(t)+4\dot{\xi}\left(t+\frac{1}{2}\,\delta t\right)+\dot{\xi}(t+\delta t)\right]+O(\delta t^5\dot{\xi}^{(4)}). \tag{A2}$$

Using Eqs. (2) and (A1) in Eq. (A2) the velocities can be eliminated to give

$$\xi(t+\delta t)=c_1\left[1+\frac{1}{2}\,\delta t\xi(t+\delta t)\right]^{-2}+c_2, \tag{A3}$$

where

$$c_1=\frac{\delta t m}{6Q}\sum_i\left[\mathbf{v}_i\left(t+\frac{1}{2}\,\delta t\right)+\frac{1}{2}\,\delta t\,\frac{\mathbf{f}_i(t+\delta t)}{m}\right]^2 \tag{A4}$$

and

$$c_2=\xi(t)+\frac{\delta t}{6}\left[\dot{\xi}(t)+4\dot{\xi}\left(t+\frac{1}{2}\,\delta t\right)-n_f k_B T/Q\right]. \quad \text{(A5)}$$

$\xi(t+\delta t)$ is iterated from Eq. (A3) when

$$\left|-c_1\delta t\ \Big/\left(1+\frac{1}{2}\,\delta t\xi\right)^3\right|<1 \quad \text{(A6)}$$

(ξ must be larger than $-2/\delta t$) or—when Eq. (A6) is not valid—from the inverse relation

$$\xi(t+\delta t)=\frac{2}{\delta t}\{[c_1/(\xi(t+\delta t)-c_2)]^{1/2}-1\} \quad \text{(A7)}$$

(ξ must be larger than c_2). The Verlet algorithms are found to be more suitable than the Gear predictor-corrector algorithms in solving Eqs. (1) and (2) because the former preserve better the time reversal symmetry of Eqs. (1) and (2).[40] We also checked that the pseudo-Hamiltonian[17–19,40] is a constant with five significant digits.

[1] J. Friedel, *Dislocations* (Addison-Wesley, London, 1954).
[2] C. Teodosiu, *Elastic Models of Crystal Defects* (Springer-Verlag, Berlin, 1982).
[3] M. P. Allen and D. J. Tildesley, *Computer Simulation of Liquids* (Clarendon, Oxford, 1987).
[4] R. M. J. Cotterill and M. Doyama, Phys. Rev. **145**, 465 (1966).
[5] V. R. Fidelman and V. A. Zhuravlev, Phys. Met. Metallogr. **46**, 85 (1979).
[6] H. Häkkinen, S. Mäkinen, and M. Manninen, Phys. Rev. B **41**, 12 441 (1990).
[7] J. Huang, M. Meyer, and V. Pontikis, Phys. Rev. B **42**, 5495 (1990).
[8] J. von Boehm and R. M. Nieminen, Phys. Scr. T **33**, 216 (1990).
[9] J. von Boehm and R. M. Nieminen, in *Many Atom Interactions in Solids*, edited by R. M. Nieminen, M. J. Puska, and M. J. Manninen, Springer Proceedings in Physics Vol. 48 (Springer-Verlag, Berlin, 1990), p. 191.
[10] J. Huang, M. Meyer, and V. Pontikis, Phys. Rev. Lett. **63**, 628 (1989).
[11] J. Huang, M. Meyer, and V. Pontikis, Philos. Mag. A **63**, 1149 (1991).
[12] R. W. Balluffi, Phys. Status Solidi **42**, 11 (1970).
[13] M. Wuttig and K. H. Birnhaum, Phys. Rev. **147**, 495 (1966).
[14] F. Ercolessi, M. Parrinello, and E. Tosatti, Philos. Mag. A **58**, 213 (1988).
[15] G. J. Ackland, G. Tichy, V. Vitek, and M. W. Finnis, Philos. Mag. A **56**, 735 (1987).
[16] J. von Boehm and R. M. Nieminen, Phys. Rev. B **50**, 6450 (1994).
[17] S. Nosé, J. Chem. Phys. **81**, 511 (1984).
[18] S. Nosé, Mol. Phys. **52**, 255 (1984).
[19] W. G. Hoover, Phys. Rev. A **31**, 1695 (1985).
[20] D. J. Evans and B. L. Holian, J. Chem. Phys. **83**, 4069 (1985).
[21] W. C. Swope, H. C. Andersen, P. H. Berens, and K. R. Wilson, J. Chem. Phys. **76**, 637 (1982).
[22] S. Toxvaerd and O. H. Olsen, Phys. Scr. T **33**, 98 (1990).
[23] J. M. Holender, Phys. Rev. B **41**, 8054 (1990).
[24] J. R. Beeler and G. L. Kulcinski, in *Interatomic Potentials and Simulation of Lattice Defects*, edited by P. C. Gehlen, J. R. Beeler, and R. I. Jaffee (Plenum, New York, 1972), p. 735.
[25] M. I. Baskes, Mater. Sci. Eng. A **108**, 289 (1989).
[26] D. M. Esterling, A. R. McGurn, I. M. Boswarva, and R. J. Arsenault, Mater. Sci. Eng. **68**, 97 (1984).
[27] D. M. Esterling and R. J. Arsenault, Mater. Sci. Eng. A **108**, 291 (1989).
[28] We have found empirically that this method gives lower values for $\mathscr{T}$ than a quasidynamic method in equal computing times.
[29] R. A. Johnson, J. Phys. F **3**, 295 (1973).
[30] N. Q. Lam, L. Dagens, and N. V. Doan, J. Phys. F **13**, 2503 (1983).
[31] Experimental data compiled in Refs. 5 and 15.
[32] R. W. Siegel, in *Point Defects and Defect Interactions in Metals*, edited by J. Takamura, M. Doyama, and M. Kiritani (University of Tokyo Press, Tokyo, 1982), p. 533.
[33] W. Schilling, J. Nucl. Mater. **64–70**, 410 (1978).
[34] The comparison between the calculated ATVF values in the bulk and the experimental values is not very meaningful because the experimental values are used as fitting parameters in the ATVF model.
[35] In Ref. 16 we reported $E_f^v=1.4$ eV for gold indicating that the vacancy formation energy increased from the value 0.962 eV in the bulk. However, the configuration in Ref. 16 was not sufficiently relaxed which caused the error.
[36] S. J. Plimpton and E. D. Wolf, Phys. Rev. B **41**, 2712 (1990).
[37] P. E. Blöchl, E. Smargiassi, R. Car, D. B. Laks, W. Andreoni, and S. T. Pantelides, Phys. Rev. Lett. **70**, 2435 (1993).
[38] G. De Lorenzi and F. Ercolessi, Europhys. Lett. **20**, 349 (1992).
[39] J. Mei and J. W. Davenport, Phys. Rev. B **42**, 9682 (1990).
[40] S. Toxvaerd, Mol. Phys. **72**, 159 (1991).